

Weakly- and Semi-Supervised Probabilistic Segmentation and Quantification of Ultrasound Needle-Reverberation Artifacts to Allow Better AI Understanding of Tissue Beneath Needles

Alex Ling Yu Hung¹, Edward Chen² and John Galeotti³

Abstract—Ultrasound image quality has been continually improving. However, when needles or other metallic objects are operating inside the tissue, the resulting reverberation artifacts can severely corrupt the surrounding image quality. Such effects are challenging for existing computer vision algorithms for medical image analysis. Needle reverberation artifacts can be hard to identify at times and affect various pixel values to different degrees. The boundaries of such artifacts are ambiguous, leading to disagreement among human experts labeling the artifacts. We propose a weakly- and semi-supervised, probabilistic needle-and-needle-artifact segmentation algorithm to separate the desired tissue-based pixel values from the superimposed artifacts. Our method models the intensity decay of artifact intensities and is designed to minimize the human labeling error. We demonstrate the applicability of the approach, comparing it against other segmentation algorithms. Our method is capable of differentiating the reverberations from artifact-free patches between reverberations, as well as modeling the intensity fall-off in the artifacts. Our method matches state-of-the-art artifact segmentation performance, and sets a new standard in estimating the per-pixel contributions of artifact vs underlying anatomy, especially in the immediately adjacent regions between reverberation lines.

I. INTRODUCTION

Ultrasound sonography is a low-cost, safe, and fast imaging technique that is widely used globally. Its real-time operation is perfect for monitoring needle insertions and other clinical interventions. However, highly reflective parallel surfaces such as needle walls can create significant reverberation artifacts because the sound wave reverberates between the posterior and anterior surfaces of the object [1]. When the amount of reflected energy is significant, it manifests as an additional echo from the same surface. The reverberation artifacts are relatively bright, looking like actual boundaries which sometimes would overlap with tissue present in the image. Not only can needles and other metallic objects cause such artifacts, certain anatomical structures with large acoustic impedance might lead to reverberation artifacts as well [2]. This kind of artifact can cloud clinicians'

judgement and confuse medical-image-analysis algorithms. For some pixels, it can be difficult to differentiate whether the pixel is an artifact, or to assign a percentage to the pixel indicating how much of the pixel's value is artifact vs actual tissue measurement. The brightness of artifacts somewhat-predictably falls off as they get further away from the reflective object, but the artifacts have uncertain boundaries and differing intensity distributions. Pixel-wise labeling is challenging and time consuming even for experts, who can have considerable differences in their annotations, an example is shown in Fig. 1. Semi-supervised approaches can reduce human labeling time, and weak supervision can estimate how much of the pixel is corrupted by the reverberation artifact.

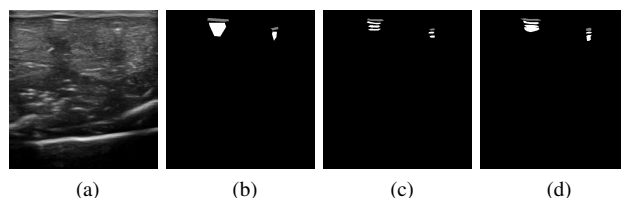


Fig. 1: Example of different labels by different annotators on the same image. Annotators disagree on the boundaries and the pixels between each reverberation.

In this paper, we proposed a novel weakly- and semi-supervised probabilistic needle-and-reverberation-artifact segmentation algorithm. The algorithm can be broken into three parts. The first part is a probabilistic segmentation network trained with hard labels. The probabilistic segmentation is used to cope with the labeling errors and ambiguity in the input images. The second part is a transform function that turns the output of the first network into soft labeled images where the value of each pixel represents how much of the pixel value is affected by the artifact. The last part is another network that is trained with the newly generated labels as desired output. The main contributions of this paper are: (1) We developed a weakly- and semi-supervised segmentation framework to segment the needle and reverberation artifact which could cope well with the insufficiency in labeled data. (2) Our probabilistic approach is able to deal with ambiguity in the artifact boundaries, and variations in human labels. (3) Our approach estimates how much of the pixel values are corrupted by reverberation artifacts.

*This present work was sponsored in part by US Army Medical contracts W81XWH-19-C0083, W81XWH-19-C0101, and W81XWH-19-C-0020, and by a PITA grant from the state of Pennsylvania DCED C000072473.

¹Alex Ling Yu Hung is with Biomedical Engineering Department, Carnegie Mellon University, Pittsburgh PA 15213, USA lingyuh@andrew.cmu.edu

²Edward Chen is with Robotics Institute, Carnegie Mellon University, Pittsburgh PA 15213, USA edward2c@andrew.cmu.edu

³John Galeotti is with Robotics Institute, Carnegie Mellon University, Pittsburgh PA 15213, USA jgaleotti@cmu.edu

II. RELATED WORK

There already exists a long history of research for developing algorithms to identify and remove reverberation artifacts from medical images. [3] produces a near optimal estimate of the reflectivity value due to reverberation by soft thresholding the 2D discrete wavelet transform. [4] improves the method proposed by [3] by utilizing radiofrequency (RF) data and soft thresholds on the wavelet coefficients to estimate the reflectivity values caused by the artifact. [5] models the reverberation mathematically, identifying and removing the artifact in RF data. Temporal information is used by [6] when they develop the 3D filter to reduce reverberation artifacts. These methods either made use of the RF data or temporal information, i.e. video sequence, but most of the times, we won't have access to RF data or a large number of ultrasound videos.

Many deep learning segmentation frameworks for medical images can be good at segmenting reverberation artifacts too, but to the best of our knowledge, there is no learning-based segmentation framework specific to reverberation artifacts in ultrasound images. U-Net [7] uses an encoder-decoder framework with skip connections between the encoder and the decoder, enabling the network to tend to more fine-grained details. [8] puts Long Short-Term Memory layers (LSTM) and U-Net together, enabling the proposed USVS-Net to excel at identifying ambiguous boundaries and be robust against speckle noises. Attention U-Net is proposed by [9] to suppress irrelevant regions and have the network focus more on the target structure with different shapes and sizes. [10] re-calibrates the channels by putting Squeeze and Excitation (SE) blocks [11] into a normal U-Net to increase the values of meaningful features and suppress the values of the insignificant ones. Together with dual attentive fusion blocks, adversarial learning is used in [12], allowing semi-supervision of the segmentation, instead of a full supervision, so that it is able to solve the problem of not having enough labeled data to some extent. These methods are robust in a fully supervised situation and are good at segmenting structures with hard labels, but they are not able to generate segmentation masks that have a meaningful probabilistic output, i.e. they are unable to model the ambiguity in the data.

[13] explicitly models the aleatoric and epistemic uncertainty in deep learning and increased the performance on noisy data sets with dropout layers and an additional variance term in the output. [14] adopts Monte Carlo dropout to explore the uncertainty in the network for medical image segmentation. This work further explains how to capture different types of uncertainty in medical images. [15] combined a conditional variational autoencoder with a U-Net. The model does not just provide a single segmentation for a given input; instead it predicts multiple plausible segmentations drawn from the distribution learned from the training data. However, this framework only works well on images with a single object or with global variations. As a result, a hierarchical probabilistic U-Net (HPU-Net) [16] is proposed

to solve such problems. Instead of global latent variables, coarse-to-fine hierarchical latent variable maps are used in this work. Besides U-Net like blocks in the decoder side, some blocks are also sampled from the prior which is trained to have similar distribution with the posterior. [17] models the conditional probability distribution of the segmentation given an input image with a network named PHiSeg. Like the HPU-Net, PHiSeg also uses a posterior network and a prior network. However, unlike the HPU-Net, the likelihood network in this work completely samples from the prior network. [18] proposed a weakly supervised framework to segment the shadows in ultrasound images. Essentially, the work uses one network for the initial segmentation, feeds the output of this network into a transform function, and then gets a new set of labels to train another network. The transform function here transforms the hard labels to soft labels, and at the same time, reduces the effect of labeling error.

III. METHOD

A. Overview

Inspired by [18], we proposed a multi-step segmentation framework, shown in Fig. 2. The entire framework could be divided into three parts: (1) a probabilistic segmentation trained on hard labels, (2) a transformation function which takes in the output of the first network and transforms the probabilistic outputs into soft labels, (3) another probabilistic segmentation network trained on the newly generated soft labels. Our algorithm differs from [18] in four main parts: (1) our transform function is designed based on the appearances and physical properties of reverberation artifacts instead of shadows, (2) we not only improve the segmentation masks in the transform function, but also quantify the artifacts, (3) we purpose to use a probabilistic segmentation to compensate for the over-labeling by human experts instead of deterministic segmentation, (4) We propose a new probabilistic segmentation network that learns variance from a known variance posterior. Even though the first part of the algorithm is fully supervised, accurate labeling is not needed since the probabilistic segmentation method models the ambiguity in the labels and the original inputs. After getting the first network trained, the unlabeled ultrasound images could be passed through the network, creating hard segmentations on the unlabeled images. The number of training data for the second network can also be increased with this approach. The output of the first network would then be modified by a transform function, which converts the hard labeled segmentation into soft labels. The transform function is designed specifically for the appearance and physical properties of reverberation artifacts in ultrasound images. The second network is designed to further eliminate the effects of uncertainty in human labels and ambiguity of the images, creating a soft labeled segmentation which represents how much of each pixel value is corrupted by the reverberation artifacts.

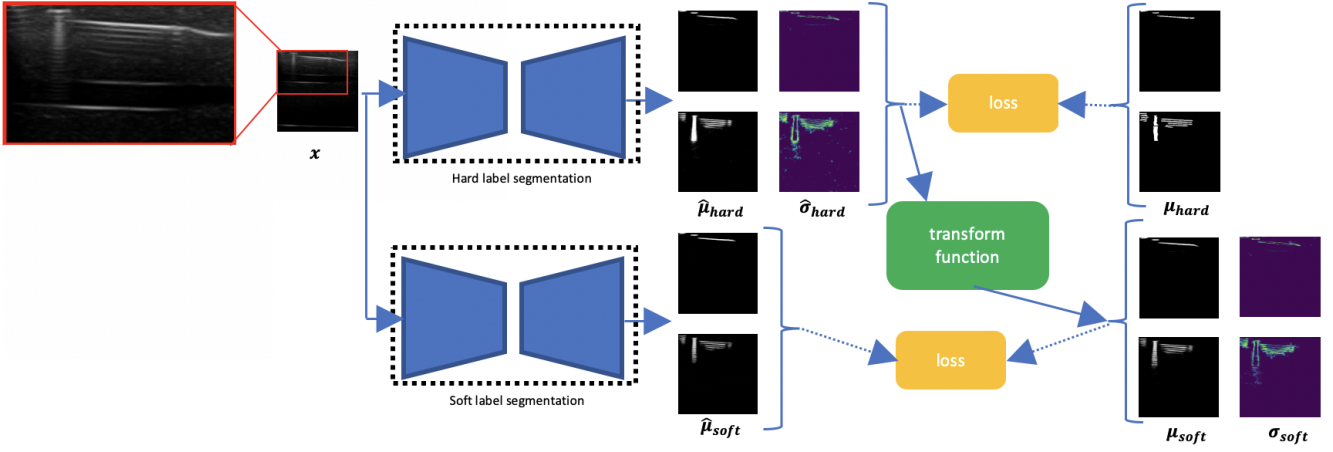


Fig. 2: The pipeline of the algorithm is inspired by [18]. However, due to the difference between reverberation artifacts and shadow artifacts, we use probabilistic networks and a novel transform function in our work.

B. Probabilistic Segmentation on Hard Labels

The artifacts might differ by shape, intensity distribution, and unclear boundaries. Therefore, the human labels could be different across different annotators. Even when the same annotator labels the same images multiple times, the results can still differ. As a result, we conjecture that careful elimination of the ambiguity in the labeling can assist with subsequent analysis. Ideally, the segmentation algorithm needs to generate nearly identical results for the same images despite using data labeled by different annotators. The work in [16] models the ambiguity in the images and the labels, which is what we look for in this stage of work. Therefore, we utilize their network for our first step: segmentation on hard labels. In our network, even though we used the same general structure as [16], we used more local blocks than global blocks, so that we could model the ambiguity of the edges better.

We train the network with hand labeled images, but after it is trained, we don't necessarily need to use the labeled training images for the following steps. Sampling from a learned distribution, the network will generate two mean maps and two standard deviation maps for the artifacts and needles segmentation. We denote these output mean maps for artifacts and needles as $\hat{\mu}_{artifact,hard}$ and $\hat{\mu}_{needle,hard}$ respectively. We denote the output standard deviation maps for artifacts and needles as $\hat{\sigma}_{artifact,hard}$ and $\hat{\sigma}_{needle,hard}$ respectively.

C. Transform Function

Even though the output of the first network inherently models the ambiguity in the input images and the human labels, it doesn't account for the fact that weaker reverberation artifacts don't affect the quality of the image as much as the strong ones do. Therefore, we transform the segmentation mask into a soft labeling mask, which models how much the artifact affects the pixel value. There are three components

to our transform function: (1) reduction of false positives, (2) introduction of an exponential decay depending on how far the artifact is relative to the needle causing the artifact, and (3) lowering the artifact-segmentation soft labels for pixels in between adjacent reverberations.

The first part of the transform function takes in predicted hard needle mask $\hat{\mu}_{needle,hard}$ and artifact mask $\hat{\mu}_{artifact,hard}$. We begin by clustering the artifacts based on distance. We then determine if there is a needle closely above a cluster of artifacts: if there is, then keep the artifacts, and set the needle as the cause this cluster of artifacts to deal with the situation where there are multiple needles in the image. If not, then remove the cluster. The pseudo-code for the algorithm is shown in Algorithm 1. The horizontal threshold ht will be small because needle artifacts are typically (near) continuous horizontal lines, whereas the vertical threshold vt will be larger to encompass the vertical spacing between artifact lines, which is based on the needle's reverberating cross section [2]. The threshold t indicates the largest possible distance between the segmented artifacts and the corresponding needles for the artifacts to be considered true positives. In this paper, for 256×256 images, we set $ht = 7$, $vt = 11$, and $t = 10$. The hyperparameters would not affect the result much as long as they are in a reasonable range.

The second part of the the transform function's purpose is to create the exponential decay in the segmentation and, at the same time, compensate for the pixels that don't comply with the decay. As sound waves travel through a medium, the intensity falls off as the distance increases. Normally, the intensity decays exponentially [19], and due to the fact that reverberation artifacts are caused by sound waves reverberating inside the tissue [1], the intensity of the reverberation artifacts should be no different. The first bounce of the sound wave at the needle represents the needle, followed by resonating bounces resulting in the artifact, so

Data: $\hat{\mu}_{needle,hard}$, $\hat{\mu}_{artifact,hard}$

Result: y_1 : artifact mask with false positives removed

$B, y_0 = \text{zeros}(\hat{\mu}_{artifact,hard}.shape); k = 1;$

for [row i , column j] *where* $\hat{\mu}_{artifact,hard}[i, j] > 0$
do

if $B[i, j] == 0$ **then**

 create stack s ;

$s.push([i, j]); B[i, j] = k$;

while s is not empty **do**

$[x, y] = s.pop$;

for $[ii, jj]$ *where* $(\frac{ii-x}{vt})^2 + (\frac{jj-y}{ht})^2 < 1$
 do

if $B[ii, jj] == 0$ **then**

$s.push([ii, jj]); B[ii, jj] = k$;

$k++$;

$set1 = \text{where}(\hat{\mu}_{needle,hard} > 0.5)$;

for ($kk = 1; kk < k; kk++$) **do**

$set2 = \text{where}(B == kk)$;

if $\exists [i_0, j_0] \in set2, [i_1, j_1] \in set1$, and

$\forall [i_2, j_2] \in set1$, s.t. i_0 below i_2 and

$\text{distance}([i_0, j_0], [i_1, j_1]) < t$ **then**

$y_1 = (B == kk) * \hat{\mu}_{artifact,hard}$

Algorithm 1: false positives removal

the intensity of the artifact should be on an exponential decay of the intensity of the needle. The intensity of the artifact falls until the bottom of the identified artifact pixels. This exponential decay can be modeled as:

$$y_{2,1}(i, j) = y_1(i, j)e^{-\alpha \frac{h(i, j)}{d(i, j)}} \quad (1)$$

where α is a hyper parameter, depending on the ultrasound machine and the mode it's in. The higher the frequency the larger α should be, as sound waves would then encounter more resistance in depth. For the experiments in this paper, $\alpha = 0.8$. Note that α should be set somewhere close to 1 to get decent results. $h(i, j)$ represents the distance of pixel (i, j) to the needle that is causing the artifact. $d(i, j)$ denotes the distance between the deepest pixel (the furthest pixel away from the corresponding needle) in the cluster of artifacts containing (i, j) and the nearest pixel in the corresponding needle.

However, other objects and tissues in the image would also have minor effects on the pixel values in the reverberation artifacts, e.g. other boundaries which overlap with the reverberation, shadows caused by vessels interacting with the reverberations, etc. The exponential-decay artifact model does not account for these other, desired, components of the pixel values. To deal with the problem, we also create an alternate measurement $y_{2,2}$ based on the pixel values in the input ultrasound images. Denote the original input ultrasound image as I . For normalization, we first find the maximum pixel value m_1 in the needle-region of I . The normalized pixel values in I can then be used as weights on the artifact

soft-label mask as follows:

$$m_1 = \max_{\forall (ii, jj), \hat{\mu}_{needle,hard}(ii, jj) > 0.5} I(ii, jj) \quad (2)$$

$$y_{2,2}(i, j) = \frac{I(i, j)}{m_1} y_1(i, j) \quad (3)$$

In cases where artifact pixels are unusually bright, e.g. $y_{2,2}$ large due to overlap with actual object boundaries, we want to preserve such property because it represents actual anatomy or a different artifact (such as a diagnostic B-line in a lung). We therefore combine $y_{2,1}$ and $y_{2,2}$ by taking the maximum

$$y_2(i, j) = \max(y_{2,1}(i, j), y_{2,2}(i, j)) \quad (4)$$

At this point, we have removed the false positives and also created an exponential decay in the artifact soft labels while preserving the effects of underlying anatomic boundaries on artifacts. However, we still need to assign lower values to the soft labels in between each reverberation, since the hard human labels tend to (incorrectly) in-paint such regions. The pixels between reverberations tend to have lower values than the artifact pixels in the original input images. In the third part of our transform function we determine whether a certain pixel belongs to the non-artifact region in between reverberation lines. We need to compare the value of that pixel in the original input ultrasound image against the maximum value in a local patch. We also apply a sigmoid-like function to make sure that artifact soft labels are limited with respect to the highest intensity value within that region.

$$m_2(i, j) = \max_{(ii, jj) \in \Omega_1(vw, hw)} I(i + ii, j + jj) \quad (5)$$

$$\mu_{artifact,soft}(i, j) = \frac{y_2(i, j)}{1 + e^{-\frac{\beta I(i, j)}{m_2(i, j)} + \frac{\beta}{2}}} \quad (6)$$

where β is a hyper-parameter that controls how fast the fall-off is. If the noise level is high, we should use a larger parameter for this. Also, $\Omega_1(vw, hw)$ is a rectangular region where $(0, 0)$ is the center point, $2vw$ and $2hw$ is the height and width. vw and hw stand for horizontal window and vertical window respectively. vw should be large enough to include at least one line of true reverberation artifact in the patch. In this paper, we set $\beta = 8$, $vw = 2$, and $hw = 1$. Again, these parameters are not sensitive, as long as vw and hw stay relatively small.

As for the standard deviation map of artifacts, we want to rescale its values in the same manner as we rescaled the mean map of artifacts. Therefore, the transform function for the standard deviation map can be simplified as

$$\sigma_{artifact,soft}(i, j) = \frac{\mu_{artifact,soft}(i, j)}{\hat{\mu}_{artifact,hard}(i, j) + \epsilon} \quad (7)$$

where $\epsilon \ll 1$ avoids division by zero.

The needle labels will not change in this part, as a result, we have $\mu_{needle,soft}(i, j) = \hat{\mu}_{needle,hard}(i, j)$, and $\sigma_{needle,soft}(i, j) = \hat{\sigma}_{needle,hard}(i, j)$.

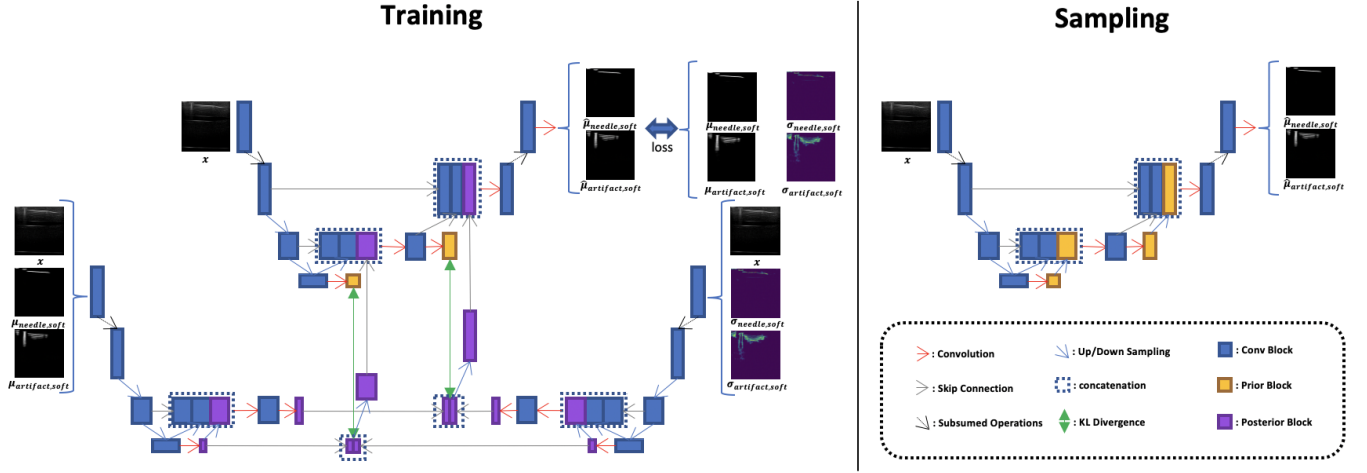


Fig. 3: Our proposed probabilistic network is similar to Hierarchical Probabilistic U-Net [16], but instead of learning the posterior with labeled segmentation masks, our method learns mean and variance of the posterior from known mean and variance separately. Therefore, two variational autoencoders are used in the posterior.

D. Probabilistic Segmentation on Soft Labels

Our segmentation model here is built upon the HPU-Net [16], and we follow their notation below. We want to model the unknown ambiguity in the images and the labels, and at the same time, we also want to take the known variance in the labels into account. Our training objective is similar to that of the previous work: maximizing the evidence lower bound on the likelihood $p(M|X)$, except that we are modeling a variational posterior $Q(\cdot|X, M, V)$ instead of $Q(\cdot|X, M)$, where X is the input image, M is the known mean of the segmentation label, and V is the variance of the segmentation label. We calculate the posterior Q from two separate networks, where one network accounts for the mean $\mu_i^{post}(z_{<i}, X, M)$ and the other network models the variance $\sigma_i^{post}(z_{<i}, X, V)$. The latents in the prior blocks should follow a normal distribution generated by the posterior blocks $N(\mu_i^{post}(z_{<i}, X, M), \sigma_i^{post}(z_{<i}, X, V))$. During training, we directly sample from the posterior Q , and train the normal distribution generated by the prior $N(\mu_i^{prior}(z_{<i}, X), \sigma_i^{prior}(z_{<i}, X))$ to be close to the one from the posterior. When sampling, we did exactly the same as the previous work did: sampling the latents from the normal distribution modeled by the prior. The training and sampling process is illustrated in Fig. 3.

In this particular application, we utilize a mean square error-based custom loss function as a way to deal with the continuous values and unique meaning of soft labels. To deal with overfitting to the background, we only care about the pixels that have values over a certain threshold γ . Lower weights are assigned to pixels where absolute error is within the known standard deviation, since we are less sure about the value in the label where standard deviation is larger.

Therefore, the loss function can be expressed as the following

$$loss = \sum_{\forall(i,j) \in \Omega_2} w(i,j) (\hat{\mu}_{soft}(i,j) - \mu_{soft}(i,j))^2 \quad (8)$$

where

$$\Omega_2 = \{(x,y) | \hat{\mu}_{soft}(x,y) > \gamma \vee \mu_{soft}(x,y) > \gamma\} \quad (9)$$

$$w(i,j) = \begin{cases} k & \text{abs}(i,j) < \sigma_{soft}(i,j) \\ 1 & \text{abs}(i,j) \geq \sigma_{soft}(i,j) \end{cases} \quad (10)$$

$$\text{abs}(i,j) = |\hat{\mu}_{soft}(i,j) - \mu_{soft}(i,j)| \quad (11)$$

and $k < 1$.

IV. EXPERIMENTS

The ultrasound imaging was performed with a UF-760AG Fukuda Denshi diagnostic ultrasound imaging machine. The imaging was done on both a chicken breast and an anthropomorphic phantom containing simulated vessels in a tissue medium produced by Advanced Medical Technologies. We used a linear transducer width 51mm scanning width. It was set to 12MHz with an imaging depth of 4cm. The gain value was 21dB. The dimension of each image is 512×532 pixels and the pixel pitch is 0.10mm horizontally and 0.075mm vertically. The images were then resized to 256×256 . The labeling in this work utilized the labeling tool Labelme [20]. The training set is over-labeled (more false positives, fewer false negatives) to show that our algorithm is good at dealing with inaccurate labels as well as handling false positives in the training data. The test set was carefully labeled such that (1) the pixels that definitely belong to needles and to the significant artifacts are segmented, (2) the pixels that are between the reverberations and not part of the artifacts are not segmented, (3) the fuzzy artifacts are segmented with lower values, and that (4) very few false positives are included in our segmentation-training soft

labels. A sample is shown in Fig. 4a, where the yellow and pink regions indicate the possible areas containing needles and artifacts respectively, green and white regions represent the first and second reverberations that we’re confident in, the bright blue circles represent the patch between reverberation with no artifacts, the dark blue are the needle patches that we’re confident in, and the red patches are the regions with identifiable fuzzy artifacts. We define the artifact pixels with values that are greater than 0.05 as positive, and needle pixels with values that are greater than 0.5 as positive.

Our notations are summarized in Table I. We denote the ratio between positive artifact and needle counts in the labeled first, second reverberations and needle and the total pixels counts in those regions as FAR (first artifact rate), SAR (second artifact rate), NR (needle rate) respectively, and the average value for positives in those artifact patches as FAA (first artifact average) and SAA (second artifact average). We also denote the false positive rate of artifacts and needles as AFPR (artifact false positive rate) and NFPR (needle false positive rate), and the average value of the false positives as AFPA (artifact false positive average) and NFPA (needle false positive average). We also calculate the average of the non-artifact region between reverberations as NAA (non-artifact average). We further define the average positive artifact value in the identifiable fuzzy artifact patches as IFAA (identifiable fuzzy artifact average).

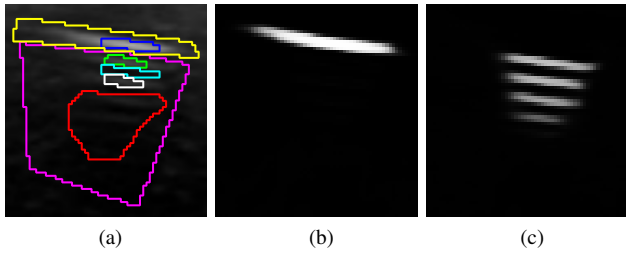


Fig. 4: Labels and segmentation results. In Fig. 4a, yellow and pink labeled areas represent the possible areas containing needles and artifacts respectively, green and white labeled regions indicate the patches that are definitely the first and second reverberations, the bright blue circle(s) represent the non-artifact patches between reverberations, the dark blue region(s) are the most confident needle pixels, and the red patches are the regions with identifiable fuzzy artifacts.

In our first experiment, we compared our results against expert labels, U-Net [7], USVS-Net [8], and HPU-Net [16] to show that our proposed algorithm is superior to these current segmentation networks and expert labels. The experts tend to label the entire region that might contain artifacts but they don’t differentiate between the reverberations. The quantitative results can be found in Table II. As can be seen in the table, our approach compares similarly to HPU-Net at binary-thresholded segmentation of the significant artifacts and needles, and our approach performs better than the other two methods. Our goal, however, is more than just binary segmentation. Since the value in the output represents how

TABLE I: Notation and Abbreviations

FAR	ratio between positive artifact pixel count in the first labeled reverberation patch and the total pixel count in the patch
SAR	ratio between positive artifact pixel count in the second labeled reverberation patch and the total pixel count in the patch
NR	ratio between needle pixel count in the labeled needle patch and the total pixel count in the patch
FAA	average output value in the first labeled reverberation patch
SAA	average output value in the second labeled reverberation patch
AFPR	false positive rate of artifacts
NFPR	false positive rate of needles
AFPA	average output value of false positive artifacts
NFPA	average output value of false positive needles
NAA	average output value of non-artifact patch between reverberations
IFAA	average output value of identifiable fuzzy artifacts

much the artifact affects the underlying “real” pixel values, and there should be a decay in the intensity of the artifacts, the average value of first artifacts should be larger than that of second artifacts. Together, they also shouldn’t be too close to 1 as they normally do not completely obscure the real tissue there. *Our method is the only algorithm that has achieved such results.* Our algorithm also limits the false positive rate to around 0.02 whereas the best results achieved by other algorithms are 0.084 and 0.04 for artifacts and needles. Our algorithm also does a good job in differentiating different reverberations, since our the average value in non-artifact patches between reverberation is 0.042, which is the lowest by far compared to 0.506, 0.431, 0.136. The IFAA value further indicates that our network learns the decay in the artifact intensity. Sample results of needle segmentation and artifact segmentation can be found in Fig. 4b and Fig. 4c. Qualitative results of artifact segmentation are shown in Fig. 5. Our method clearly does the best in differentiating the actual artifacts and the patches around them while simultaneously assigning lower values to less significant artifacts.

TABLE II: Comparison of our Entire Approach Against Other Algorithms and Expert Labels

	expert labels	ours	U-Net	USVS-Net	HPU-Net
FAR	0.966	0.986	0.978	0.859	0.996
SAR	0.993	0.994	1.0	0.976	1.0
NR	0.939	0.981	0.854	0.786	0.966
FAA	0.922	0.728	0.806	0.589	0.894
SAA	0.975	0.698	0.928	0.831	0.936
AFPR	0.129	0.022	0.237	0.168	0.084
NFPR	0.119	0.018	0.058	0.329	0.040
AFPA	0.934	0.151	0.352	0.261	0.130
NFPA	0.914	0.627	0.715	0.750	0.716
NAA	0.423	0.042	0.506	0.431	0.136
IFAA	0.990	0.471	0.871	0.836	0.775

Our second experiment is done to show that our proposed second network in the pipeline works better than other networks. In this experiment, we test out U-Net, HPU-Net,

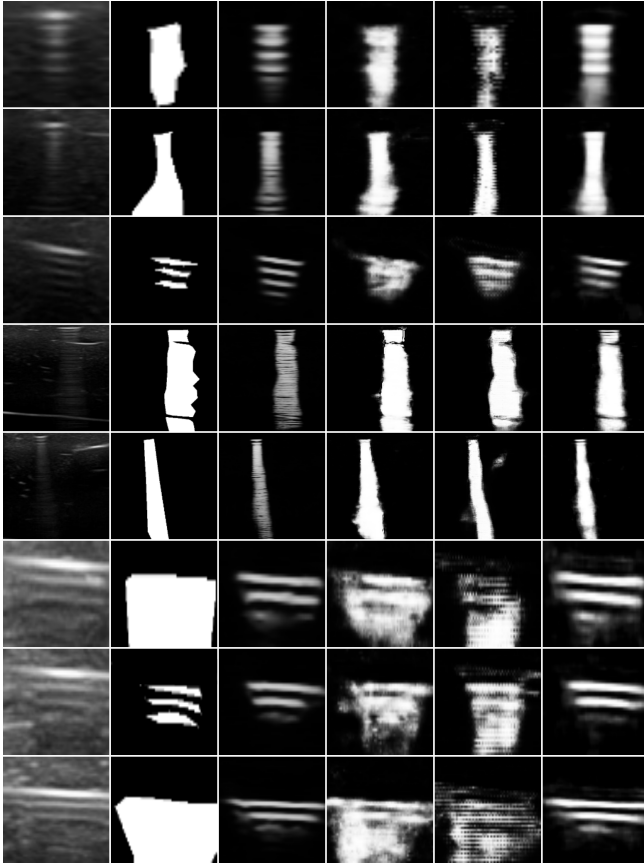


Fig. 5: Results comparison, the first five rows are images on phantom data, last three rows are images on chicken breast data. From left to right: input images (zoomed in), expert labels, our results, U-Net, USVS-Net, HPU-Net. Notice that our method differentiates the reverberations better, produces fewer false positives, picks up unlabeled artifacts and at the same time, models the exponential decay of artifact intensity.

and USVS-Net as the second network. However, USVS-Net overfits to the background too much, so it is not included in the quantitative comparison. The quantitative evaluation can be found in Table III. It shows that our method is as good as HPU-Net in detecting the strong artifacts and needles, since FAR, SAR and NR are similar. It also illustrates that our method works better in differentiating the artifacts and the patches between reverberations as well as giving higher values to the first reverberation than to the second. Lastly, our methods also produce fewer false positives and have lower values in the false-positive patches.

Our next experiment is to show that we can further improve our results with additional unlabeled data, and that if the training data of the first network is unavailable, using only non-labeled data also wouldn't hurt the performance much. The comparison can be found in Table IV, where it shows that using both labeled and unlabeled data slightly decreases the false positives of needles, and also lowers the values between reverberations. On the other hand, using only

TABLE III: Comparison of our Second Network Against Other Soft-Label Probabilistic Networks

	ours	U-Net	HPU-Net
FAR	0.986	0.978	0.986
SAR	0.994	1.0	1.0
NR	0.981	0.855	0.990
FAA	0.728	0.806	0.685
SAA	0.698	0.928	0.686
AFPR	0.022	0.237	0.060
NFPR	0.018	0.058	0.066
AFPA	0.151	0.352	0.151
NFPA	0.627	0.715	0.725
NAA	0.042	0.506	0.064
IFAA	0.471	0.871	0.476

unlabeled data only produces slightly more false positives.

TABLE IV: Benefit from Adding Labeled or Unlabeled Data

	labeled only	both	unlabeled only
FAR	0.986	0.988	0.971
SAR	0.994	0.999	0.996
NR	0.981	0.966	0.941
FAA	0.728	0.723	0.698
SAA	0.698	0.695	0.691
AFPR	0.022	0.029	0.043
NFPR	0.018	0.005	0.024
AFPA	0.151	0.143	0.125
NFPA	0.627	0.624	0.643
NAA	0.042	0.033	0.040
IFAA	0.471	0.440	0.497

To provide further validation of our algorithm on different sets of plausible hand labels, we apply aleatoric uncertainty maps obtained from a Monte Carlo dropout-based Bayesian 3-D convolutional neural network similar to [21]. In doing so, we are able to simulate the wave-like intensity decrease of needle artifacts in a realistic manner. For modeling the aleatoric uncertainty in the artifact segmentation region, we apply the model estimator as

$$\frac{1}{T} \sum_{t=1}^T \text{diag}(\hat{p}_t) - \hat{p}_t^{\otimes 2} \quad (12)$$

using the notation from [21], where $\hat{p}_t = p(\hat{w}_t)$ represents softmax outputs evaluated with a set of network weights w . In an attempt to obtain more articulate hand labels, we apply the following steps on top of our hand labels: (1) use the labels to mask only the relevant regions in the aleatoric uncertainty map, (2) take the inverse of the uncertainty map, and (3) determine a local threshold a_{thresh} for smaller patches within each labeled region and use that for deciding whether to keep or remove the labels. A sample of the aleatoric uncertainty map and uncertainty-pruned label are shown in Fig 6. We compare the results from networks trained on the original hand labels against the ones trained on the refined labels. The results are shown in Table V. Our algorithm still does a decent job on the refined labels, even though the performance is slightly worse than on original hand labels. The intuition is that although the uncertainty-pruning removes some of the labels in the spaces between

reverberations, our algorithm is designed to differentiate the reverberations from the spaces between reverberations, so it doesn't make much difference in that regards. However, the refinement step removes some of the true positives as well, which could not be learned in the networks, slightly hurting the performance. With that being said, the algorithm still does a decent job on a different set of labels.

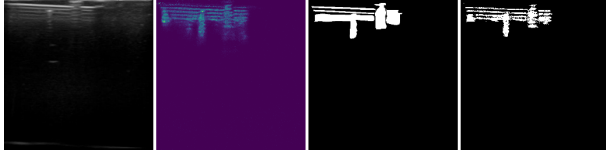


Fig. 6: Example of aleatoric uncertainty map and the uncertainty-pruned label, from left to right: input image, aleatoric uncertainty map, hand label, uncertainty-pruned label

TABLE V: Our Robustness Across Various Binary Labels

	hand labels	uncertainty-pruned labels
FAR	0.986	0.958
SAR	0.994	0.997
NR	0.981	0.955
FAA	0.728	0.630
SAA	0.698	0.668
AFPR	0.022	0.063
NFPR	0.018	0.034
AFPA	0.151	0.137
NFPA	0.627	0.621
NAA	0.042	0.044
IFAA	0.471	0.400

V. CONCLUSION

Our proposed algorithm outperforms other existing segmentation algorithms in segmenting and quantifying reverberation artifacts. Our weakly- and semi-supervised reverberation segmentation framework is able to take in inaccurate human labels and predict accurate segmentations as well as estimate how much the artifacts affect the pixel values. Our probabilistic outputs could potentially be used in compounding, ultrasound image certainty measurements, ultrasound image quality evaluation, reverberation artifacts removal etc. Also, this algorithm is directly related to robot-controlled needle insertion, in which our work can be used to guide where to insert the needle, monitor the tissue under the needle, and determine the quality of the image.

ACKNOWLEDGMENT

We would like to thank our collaborators at the University of Pittsburgh, Triton Microsystems, Inc., Accipiter Systems, Inc., Sonivate Medical, Inc., and URSUS Medical, LLC.

REFERENCES

- [1] M. Ziskin, D. Thickman, N. Goldenberg, M. Lapayowker, and J. Becker, "The comet tail artifact." *Journal of Ultrasound in Medicine*, vol. 1, no. 1, pp. 1–7, 1982.
- [2] R. M. Kirberger, "Imaging artifacts in diagnostic ultrasound—a review," *Veterinary Radiology & Ultrasound*, vol. 36, no. 4, pp. 297–306, 1995.
- [3] P. C. Tay, S. T. Acton, and J. Hossack, "A transform method to remove ultrasound artifacts," in *2006 IEEE Southwest Symposium on Image Analysis and Interpretation*. IEEE, 2006, pp. 110–114.
- [4] P. C. Tay, S. T. Acton, and J. A. Hossack, "A wavelet thresholding method to reduce ultrasound artifacts," *Computerized Medical Imaging and Graphics*, vol. 35, no. 1, pp. 42–50, 2011.
- [5] K. K. Win, J. Wang, C. Zhang, and R. Yang, "Identification and removal of reverberation in ultrasound imaging," in *2010 5th IEEE Conference on Industrial Electronics and Applications*. IEEE, 2010, pp. 1675–1680.
- [6] N. E. Bylund, M. Andersson, and H. Knutsson, "Interactive 3d filter design for ultrasound artifact reduction," in *IEEE International Conference on Image Processing 2005*, vol. 3. IEEE, 2005, pp. III–728.
- [7] O. Ronneberger, P. Fischer, and T. Brox, "U-net: Convolutional networks for biomedical image segmentation," in *International Conference on Medical image computing and computer-assisted intervention*. Springer, 2015, pp. 234–241.
- [8] T. S. Mathai, V. Gorantla, and J. Galeotti, "Segmentation of vessels in ultra high frequency ultrasound sequences using contextual memory," in *International Conference on Medical Image Computing and Computer-Assisted Intervention*. Springer, 2019, pp. 173–181.
- [9] O. Oktay, J. Schlemper, L. L. Folgoc, M. Lee, M. Heinrich, K. Misawa, K. Mori, S. McDonagh, N. Y. Hammerla, B. Kainz, *et al.*, "Attention u-net: Learning where to look for the pancreas," *arXiv preprint arXiv:1804.03999*, 2018.
- [10] A. G. Roy, N. Navab, and C. Wachinger, "Concurrent spatial and channel 'squeeze & excitation' in fully convolutional networks," in *International conference on medical image computing and computer-assisted intervention*. Springer, 2018, pp. 421–429.
- [11] J. Hu, L. Shen, and G. Sun, "Squeeze-and-excitation networks," in *Proceedings of the IEEE conference on computer vision and pattern recognition*, 2018, pp. 7132–7141.
- [12] L. Han, Y. Huang, H. Dou, S. Wang, S. Ahamad, H. Luo, Q. Liu, J. Fan, and J. Zhang, "Semi-supervised segmentation of lesion from breast ultrasound images with attentional generative adversarial network," *Computer Methods and Programs in Biomedicine*, vol. 189, p. 105275, 2020.
- [13] A. Kendall and Y. Gal, "What uncertainties do we need in bayesian deep learning for computer vision?" in *Advances in neural information processing systems*, 2017, pp. 5574–5584.
- [14] T. Nair, D. Precup, D. L. Arnold, and T. Arbel, "Exploring uncertainty measures in deep networks for multiple sclerosis lesion detection and segmentation," *Medical image analysis*, vol. 59, p. 101557, 2020.
- [15] S. Kohl, B. Romera-Paredes, C. Meyer, J. De Fauw, J. R. Ledsam, K. Maier-Hein, S. A. Eslami, D. J. Rezende, and O. Ronneberger, "A probabilistic u-net for segmentation of ambiguous images," in *Advances in Neural Information Processing Systems*, 2018, pp. 6965–6975.
- [16] S. A. Kohl, B. Romera-Paredes, K. H. Maier-Hein, D. J. Rezende, S. Eslami, P. Kohli, A. Zisserman, and O. Ronneberger, "A hierarchical probabilistic u-net for modeling multi-scale ambiguities," *arXiv preprint arXiv:1905.13077*, 2019.
- [17] C. F. Baumgartner, K. C. Tezcan, K. Chaitanya, A. M. Hötker, U. J. Muehlmatter, K. Schawkat, A. S. Becker, O. Donati, and E. Konukoglu, "Phiseg: Capturing uncertainty in medical image segmentation," in *International Conference on Medical Image Computing and Computer-Assisted Intervention*. Springer, 2019, pp. 119–127.
- [18] Q. Meng, M. Sinclair, V. Zimmer, B. Hou, M. Rajchl, N. Toussaint, O. Oktay, J. Schlemper, A. Gomez, J. Housden, *et al.*, "Weakly supervised estimation of shadow confidence maps in fetal ultrasound imaging," *IEEE transactions on medical imaging*, vol. 38, no. 12, pp. 2755–2767, 2019.
- [19] V. R. Amin, "Ultrasonic attenuation estimation for tissue characterization," 1989.
- [20] K. Wada, "labelme: Image Polygonal Annotation with Python," <https://github.com/wkentaro/labelme>, 2016.
- [21] B. J. K. Yongchan Kwon, Joong-Ho Won and M. C. Paik, "Uncertainty quantification using bayesian neural networks in classification: Application to ischemic stroke lesion segmentation," in *Conference on Medical Imaging with Deep Learning*, 2018.